DOI: 10.1595/147106704X5942

Iridium-Based Hexacyanometallate Thin Films in Aqueous Electrolytes

SOME OF THEIR ELECTROCHEMICAL AND CATALYTIC BEHAVIOURS

By Kasem K. Kasem* and Leslie Huddleston

Department of Natural, Mathematical and Information Sciences, Indiana University Kokomo, Kokomo, IN 46904-9003, U.S.A.

*E-mail: kkasem@iuk.edu

Thin films of metal-hexacyanoiridium(III) (MHCI), $K_xM_y[Ir(CN)_6]_z$, where M = Ru, Fe were electrochemically prepared and used as surface modifiers for glassy carbon electrodes. The redox behaviour of the counter/central ions of these films was investigated in aqueous electrolytes using cyclic voltammetry, chronocoulometry and electrochemical impedance spectroscopy. An electrochemical synthesis of zeolite-like films of $K_xM_y[Ir(CN)_6]_z$ and $K_xFe_y[Fe(CN)_6]_z$ (Prussian blue) was also undertaken using the cyclic voltammetric technique. Porous multi-film assemblies of Prussian blue and MHCI were formed either by the direct electrodeposition of Prussian blue over MHCI or Prussian blue over MHCI during repetitive potential cycling, or by electrochemically-driven insertion-substitution methods. In acidic aqueous KCl, iron hexacyano iridate (FeHCI) displays two redox waves with formal potential $E^o_f \approx 0.35$ and 0.6 V vs. Ag/AgCl. The electrochemical behaviour of FeHCI was compared with that of related hexacyanometallate compounds, such as $KRu_x[Ru(CN)_6]_y$, $KRu_x[Fe(CN)_6]_y$ and $KFe_x[Fe(CN)_6]_y$. In addition, evidence for the catalytic behaviour of MHCI films towards the reduction of iodate, IO_3^-, is reported.

Immobilised mixed-valence hexacyanometallates (HCM) or hexahalometallates, for example $KFe_x[Fe(CN)_6]_y$ or $M\ X_6^{-y}$, respectively, (where X = Cl, Br, M = iron (Fe), iridium (Ir), ruthenium (Ru), etc. and y is the charge) and related compounds are an important class of polynuclear compounds. Their ability to form a conducting polymer that resembles zeolitic or intercalation material, as well as redox organic polymers, has attracted the attention of many investigators (1–15). Prussian blue is an excellent example of an HCM compound. Earlier studies of Prussian blue were carried out more than two decades ago (2, 4) and substantiate the interest in further research of related compounds. As transition metals with different formal oxidation states occupy the counter ion and the central ion sites, different redox centres are created within host thin films.

Two major characteristics of this class of inorganic redox film promote its usefulness for possible applications:

- first, the oxidation or reduction of these solid films can proceed without dissolution of the solid compound as the film maintains its neutrality by an ion diffusion process, and
- second, the formation of a bi- or multilayered structure is possible using an insertion-substitution mechanism.

Hexacyanometallates also possess these characteristic features of redox active solid films. The composition, thickness and structure of HCM thin films can also be manipulated to serve a desired use and to expand some features that can be used in industrial applications. Multilayered (8–10) insoluble films of HCM have important applications in membrane chemistry. Some of the studies cited here focus on the preparation of multilayered films, carried out either by electrodeposition of one film over the other, or by mechanical mixing of two insoluble HCMs.

In addition, several studies have been carried out on HCMs in which the central atoms were Ru (16–19), cobalt (1), nickel (12), vanadium (20) or chromium (21). A limited number of studies

(22–25) have been performed on $K_x[Ir(CN)_6]_y$, but with no mention of the redox behaviour of this compound. Like most of the platinum metals, iridium oxide shows great electrocatalytic activity. This indicates that iridium compounds possess promising features as electron acceptors/donors or depolarisers in biological membranes, and more investigations are needed to understand the redox behaviour of Ir-based HCMs.

This paper reports new studies into the electrochemical behaviour of multilayered film assemblies where iron and iridium are the redox centres in $KM_x[Ir(CN)_6]_y$. Furthermore, as ruthenium hexacyanoferrate has a zeolite-like structure (26), $KFe_x[Ir(CN)_6]_y$ deposits are expected to have similar structure. An alternate method for the preparation of zeolite-like multifilm assemblies of iridium-based HCMs with bi-, or trivalent cations substituted as counter ions is discussed. Evidence for the catalytic activities of these assemblies on the electrode surfaces is presented.

Instrumentation and Methods

Experiments were carried out using a conventional three-electrode type electrochemical cell. The reference electrode was a Ag/AgCl (saturated KCl) half-cell of potential –45 mV vs. SCE. The counter (auxiliary) electrode was a platinum (Pt) wire, and the working electrode was a glassy carbon disk electrode (GCE) of surface area 0.071 cm^2. The working electrode was cleaned by polishing with 1 μm α-alumina paste and rinsed with water and acetone prior to use. An electrochemical analyser was used to perform the electrochemical studies and X-ray photoelectron spectra (XPS) with typical depth analysis of 5–50 Å were recorded. The deposited films on the electrode surfaces were examined by scanning electron microscopy.

Impedance Measurement: Electrochemical impedance spectroscopy (EIS) studies were carried out. Faradic impedance measurements were performed within a frequency range of 0.1 mHz to 1 kHz. The current response was monitored and the data were analysed by a Fourier transformation algorithm.

Chronocoulometry: Experiments were performed with pulses of width 50 ms. All the electrochemical experiments were carried out by deoxygenation in a nitrogen (N_2 99.99%) atmosphere at room temperature (25.1°C).

Electrode Modification: Thin solid films of $KFe_x[Ir(CN)_6]_y$ were electrodeposited via oxidative electropolymerisation on the glassy carbon electrode surfaces by repetitive potential cycling of a GCE between –0.30 and +1.2 V vs. Ag/AgCl, in freshly prepared aqueous solutions containing an equiv. 0.5 mM of $K_3[Ir(CN)_6].2H_2O$, either $FeCl_3$ or $RuCl_3$, and 40 mM KCl (pH 2). Scans were carried out at a sweep rate of 100 mV s^{-1}. The electrodes were then rinsed thoroughly and transferred to reactant-free electrolyte where their electrochemical response was examined. The electrode surface coverage (Γ) of this thin film was determined by integrating the areas under the voltammetric i-E curves.

A sheathing (overlaying) procedure was used to form a multifilm assembly. This included depositing $K_xFe_y[Ir(CN)_6]_z$ on the electrode surface to form the inner layer followed by deposition of $K_xFe_y[Fe(CN)_6]_z$ over the modified electrode using a similar method to that used to deposit the inner layer.

Results and Discussion

Electrodeposition of $KFe_x^{III}[Ir^{III}(CN)_6]_y$

Evidence of formation of $KFe_x^{III}[Ir^{III}(CN)_6]_y$ can be detected from the cyclic voltammograms shown in Figure 1 for the GCE in aqueous solutions containing equiv. 0.5 mM of $K_3[Ir(CN)_6].2H_2O$, and $FeCl_3$ and 40 mM of KCl (pH 2). The growth of the redox wave as successive scanning took place is indicative of the build-up of redox potential film. Notice that the anodic current is always greater than the cathodic current. Such behaviour can be attributed to the difference in the kinetics of the oxidation and reduction processes in the film.

Rate of $K^+Fe_x^{II}[Ir^{III}(CN)_6]_y$ Deposition

The slope of the plot of i_{pa} (anodic peak current) vs. the number of cycles as a function of time (Figure 1A) averages 1.04×10^{-6} μC/cycle. Considering the effective time of deposition per cycle is 2 seconds, the rate of film build up is 0.52 μC s^{-1}. This rate is equivalent to a surface coverage

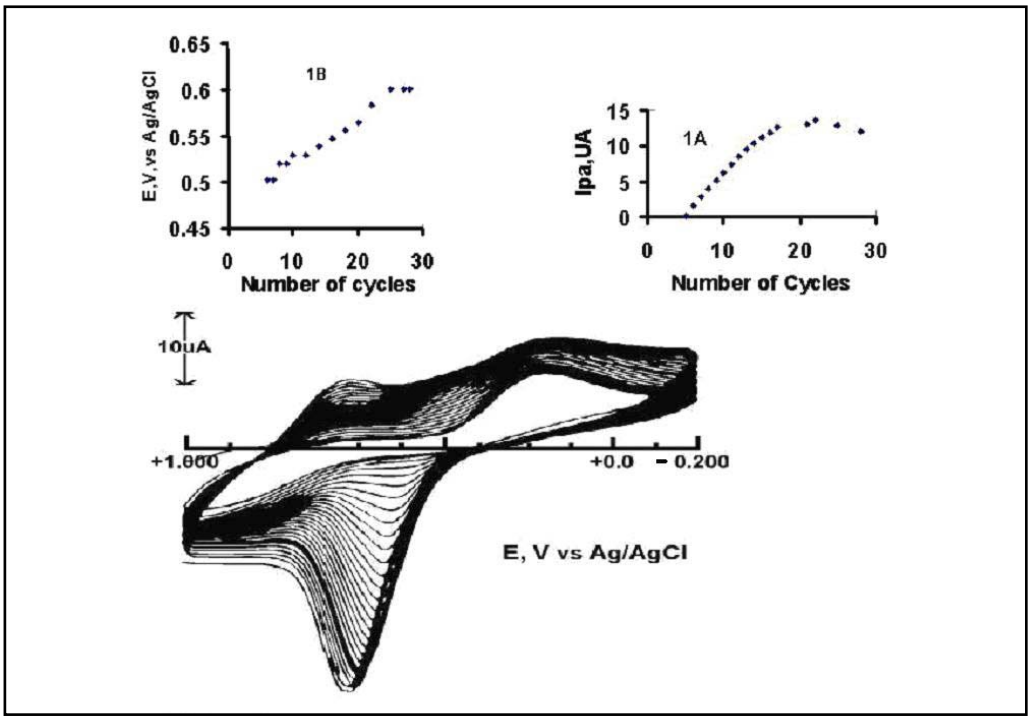

Fig. 1 Repetitive cyclic voltammetry at 0.1V s^{-1} of a glassy carbon electrode (GCE) in equivalent 1 mM of $K_3[Ir(CN)_6]$ and $FeCl_3$ in 50 mM KCl/HCl (pH = 2). Scan started at –0.20 V vs. Ag/AgCl
*1**A** Plot of anodic peak current (i_{pa}) vs. number of cycles*
*1**B** Anodic peak potential (E_{pa}) vs. number of cycles*

of 7.7 × 10^{-11} mol cm^{-2}/cycle. Figure 1A also shows that i_{pa} reached a maximum after 17 cycles and then became steady. This suggests that 20 cycles are enough to make a stable film with better mechanical properties than thicker films.

Structure of $KFe_x^{III}[Ir^{III}(CN)_6]_y$

Because of the small difference in radius among transition metal ions, calculation of the unit cell dimensions was performed as previously described in the literature (9). The calculated unit cell dimensions suggest that the monolayer thickness is ≈ 10.4 Å. This corresponds to a molar volume of 677.16 cm^3 mol^{-1}. The calculated monolayer equivalence based on the dimension of 10.4 Å is 10.75 × 10^{-10} mol cm^{-2}. Accordingly, this means that approximately 14 cycles are needed to cover the electrode surface with the first layer.

The effect of this structure on the interfacial potential between the modified electrode and the solution is demonstrated in Figure 1B which shows an irregular-linear relationship between the recorded anodic peak potential and the number of cycles up to 25 cycles, after which it maintains constant value. Such behaviour indicates that the electrode/electrolyte interface was in steady change and reached constant structure after 25 cycles. This causes multi-interface systems, consisting of native GCE/$[Ir(CN)_6]^{3-}$ and immobilised $[Ir(CN)_6]^{3-}$/free $[Ir(CN)_6]^{3-}$, to coexist. However, after the first 14 cycles the surface coverage of immobilised $[Ir(CN)_6]^{3-}$ was sufficient to create one monolayer structure of immobilised $[Ir(CN)_6]^{3-}$. This monolayer was insufficient to create an interface that would give steady current and potential (Figures 1B and 1A) as both the current and potentials kept changing.

The steady rise in the current, see Figure 1A, could be evidence for film porosity, as a one monolayer film allowed redox ions through its network structure to be in contact with the active sites on the native electrode surface.

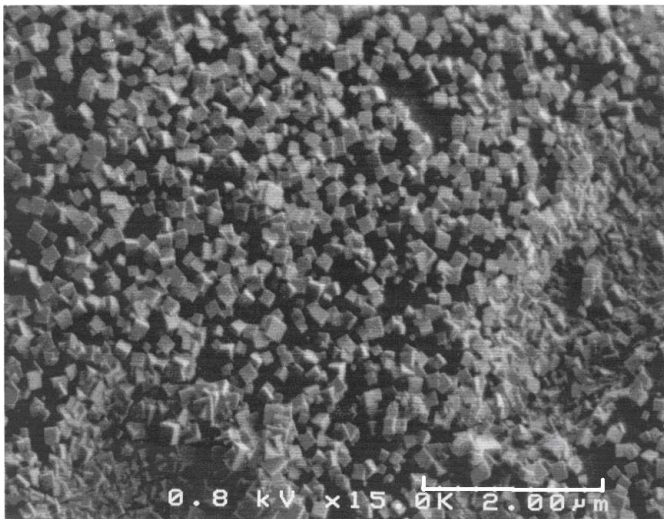

Fig. 2 Scanning electron micrograph of polynuclear hexacyanoiridium(III) films on a GCE surface. The accelerating voltage is 0.8 kV

Spectroscopic Characterisation

Figure 2 is a scanning electron micrograph of the film formed on the GCE substrate. Figure 2 shows a highly crystalline deposit of cubic shape with dimensions of ~ 200 nm. The discontinuity of this crystalline structure as well as its disordered packing makes film porosity highly likely. The XPS spectrum of the film formed (Figure 2) is shown in Figure 3. In Figure 3, the peaks corresponding to the trivalent iridium are identifiable by several peaks between 60 and 66 eV, at 105 eV, and between 300 and 500 eV. In particular, the signals at 495 eV support the Ir-O bonding that can be attributed to Ir(III) being surrounded by 6 O atoms. However, signals appearing between 705 and 725 eV indicate mixed valence Fe atoms coordinated with oxygen (Fe-O). This is evidence for the coexistence of Fe(II)-O and Fe(III)-O. The peak at 290 eV corresponds to C in the CN group, while the N peak is at 400 eV. It has been previously reported that multivalent oxides of transition metals can be codeposited from cyanometallate solutions at pH 2 (1, 27).

Redox Behaviour of $KFe_x^{III}[Ir^{III}(CN)_6]_y$ Films

The general formula of hexacyanometallates (HCMs) can be written as $MM_A^X[M_B^Y(CN)_6]_Z$; M represents main group metals, while M_A^X and M_B^Y are generally transition metals. The reduction of

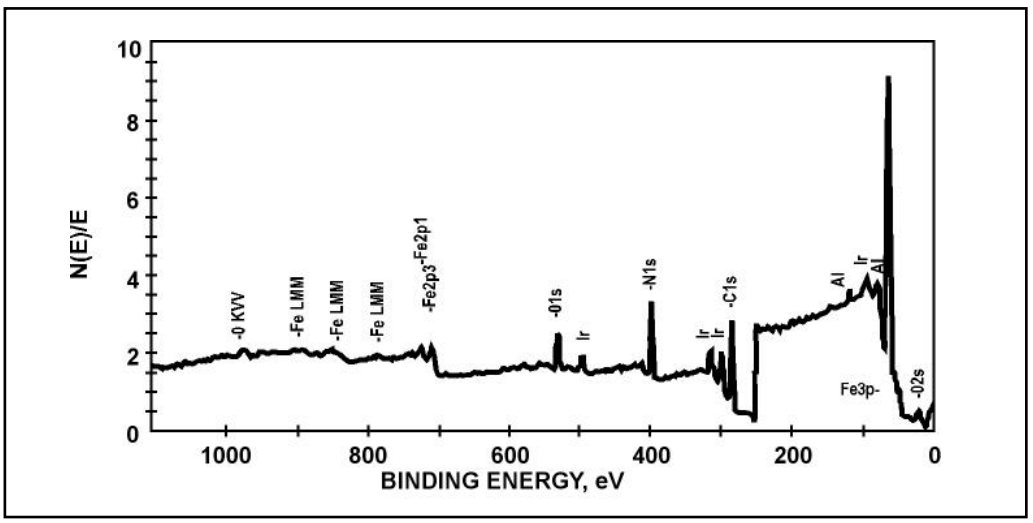

Fig. 3 X-ray photoelectron spectra (XPS) showing the binding energies and intensities of peaks of the aggregates shown in Figure 2

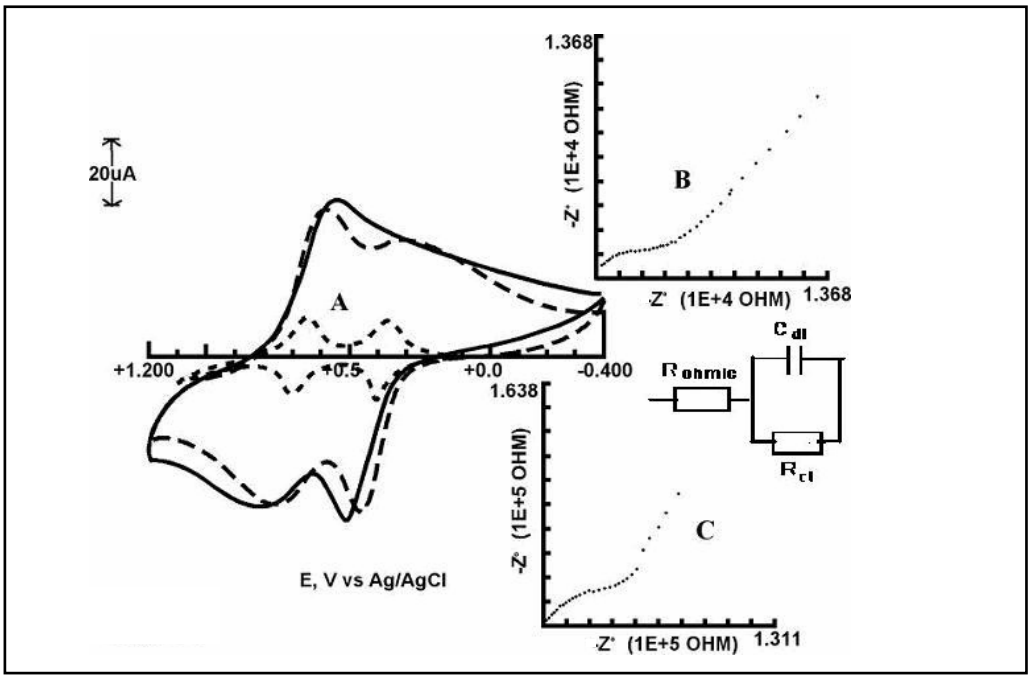

*Fig. 4**A** Cyclic voltammogram of a GCE modified with $K_xFe_y[Ir(CN)_6]_z$ in 50 mM KCl/HCl at scan rates: 0.05 V s^{-1} (----); 0.50 V s^{-1} (**----**); 0. 200 V s^{-1} (—)*
*4**B** Nyquist plot at 0.7 V; 4**C** Nyquist plot at 0.5 V*
Units: (1E+5 ohm) = 1×10^5 ohm; (1E+4 ohm) = 1×10^4 ohm

the fixed counter cations of these compounds can take place via electron/cation addition according to the Equation:

$$M_A^X[M_B^Y(CN)_6]_Z + 1e + M^+ \rightarrow MM_A^{X-1}[M_B^Y(CN)_6]_Z \quad (i)$$

while oxidation of the central atom can take place by electron loss followed by the anion addition needed for charge balance without affecting the coordination number/sphere (2):

$$M_A^X[M_B^Y(CN)_6]_Z - 1e + X^- \rightarrow M_A^X[M_B^{Y+1}(CN)_6X]_Z \quad (ii)$$

As the deposited redox centres are totally immobilised, the charge transfer process is controlled by the mobility of the K or Cl ions (from the supporting electrolyte) and by electron hopping.

Scanning the potential of a GCE, modified with $KFe_x^{III}[Ir^{III}(CN)_6]_y$ at 200 mV s^{-1} between –0.40 and 1.20 V in 0.1M KCl, produced the solid line cyclic voltammogram shown in Figure 4. The cathodic scan (upper part) shows a broader reduction peak at 0.520 V, while two anodic peaks (lower part) at 0.520 and 0.80 V are shown in the anodic scan. Such behaviour depends on the scan rate. The dotted and dashed cyclic voltammogram in Figure 4 indicates that by decreasing the scan rate both the reduction and oxidation peaks become well defined. Notice that the reduction of Fe(III) as a counter ion becomes more identifiable at a lower scan rate. Unlike the formal redox wave reported for immobilised iron hexacyanoruthenate, $K_xFe_y[Ru(CN)_6]_z$ (7), the formal redox wave of iron counter ions appears at a more positive potential (~ 0.375 V) and at a very low scan rate. Furthermore, the formal potential of the central Ir atom in the $[Ir(CN)_6]^{3-}$ redox wave was at ~ 0.680 V which is 100 mV less positive than that reported for $IrCl_6^{3-}$ (28).

The phenomena of such ill-defined redox waves in $KFe_x^{III}[Ir^{III}(CN)_6]_y$ at scan rates faster than 10 mV s^{-1} distinguish it from other studied HCM. Figure 4 shows at scan rates faster than 10 mV s^{-1}, that total overlapped waves having a formal redox centre closer to that of the central Ir ion

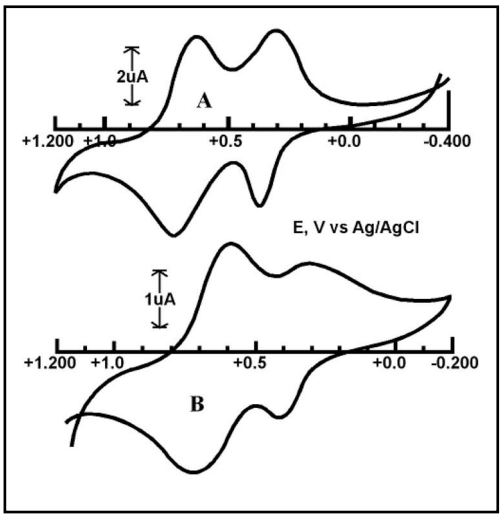

Fig. 5A Cyclic voltammogram at 0.05 V s^{-1} of a GCE modified with $K_xFe_y[Ir(CN)_6]_z$ in 50 mM KCl/HCl
5B Cyclic voltammogram after the GCE was immersed in Cu^{2+} for 120 minutes

occur. This indicates there is slow charge transfer in the counter Fe ion centre. Obtaining a well-defined Fe redox wave at (~ 0.375 V) at a slow scan rate confirms this conclusion. The fact that the compact (3*d*) orbital in Fe has less metal-donor atom bonding than the more expanded (5*d*) orbital in the Ir ion makes Ir ions soft acids. Unlike the Ru in $K_xFe_y[Ru(CN)_6]_z$ no Ir oxides are being formed. The fact that $K_xFe_y[Ru(CN)_6]_z$ shows similar electrochemical behaviour to $K_xFe_y[Fe(CN)_6]_z$, but different to that of $KFe_x^{III}[Ir^{III}(CN)_6]_y$ may indicate the effect of expanded (5*d*) orbitals in the Ir ions.

The Nyquist plots, which predict the stability and performance of a closed-loop system by observing its open-loop behaviour, see Figures 4B and 4C for a 1.49 nm film, show combined diffusional behaviour (mass transfer is the significant factor) with no sign of charge saturation, and a kinetically controlled charge transfer process. The greater Z in Figure 4C (at 0.5 V) compared to that in Figure 4B (at 0.7 V) reflects the importance of Cl^- ions in charge balance when both iron and iridium are in their highest stable oxidation states. However, when impedance measurements are carried out at 0.5 V, only the counter ion Fe is oxidised (d^5 Fe^{3+}). As the counter ion occupies the interstitial sites of octahedral $[Ir(CN)_6]_3$, the charge balance to these sites requires the removal of K^+ ions and the diffusion of Cl^- ions. The kinetics of this process may affect the magnitude of the impedance measured at this potential. The equivalent circuit for the film assembly can be pictured as an ohmic resistance (R_Ω) in series with a paralleled double layer capacitor (C_{dl}) with charge transfer resistance (R_{ct}), see inset in Figure 4. At 0.7 V, when both the Ir and Fe cations involved in the network structure of this assembly are in their highest oxidation states, the number of K^+ ions needed for charge balance in the film assembly is reduced. This will hinder self diffusion in the film. Calculations from the impedance measurement showed that the diffusion coefficent (D_{ct}) was 2.2 $\times$ 10^{-9} cm^2 s^{-1}. This quantity is in agreement with D_{ct} determined for $IrCl_6^{2-}$or $[Fe(CN)_6]^{3-}$ immobilised in poly $Ru(vbpy)_3^{2+}$ at the saturation level where the ratio of surface coverage of M (Γ_M) to that of the polymer (Γ_{Poly}) is ($\Gamma_M/\Gamma_{Poly} \geq 0.3$) (29).

Stability of $KFe_x[Ir(CN)_6]_y$ Film

Cu^{2+}-Substituted $KFe_x[Ir(CN)_6]_y$

GCEs modified with a thin film of $KFe_x[Ir(CN)_6]_y$ undergo structural alteration by substitution of the counter Fe^{3+} ion by Cu^{2+} (d^9). This is achieved by cycling the potential of the GCE modified with $KFe_x[Ir(CN)_6]_y$ thin film in the desired metal ion acidic solution. The results, see Figures 5A and 5B, indicate that Cu^{2+} partially substituted the Fe counter ions in the film.

Figures 5A and 5B show the redox wave of the film after 2 hours of Cu substitution (Figure 5B). This has not only affected the Fe redox wave, but has also decreased the total amount of redox active materials by ~ 25% of the initial amount. Unlike Prussian blue, which is fully substituted in under 2 hours, $KFe_x[Ir(CN)_6]_y$ is less susceptible to substitution.

Formation of Zeolite-Like Bilayer Film Assembly

Formation of Multi-Film Assemblies

The sheathing method previously described was performed and the results are shown in Figure 6. Figure 6A shows the cyclic voltammogram

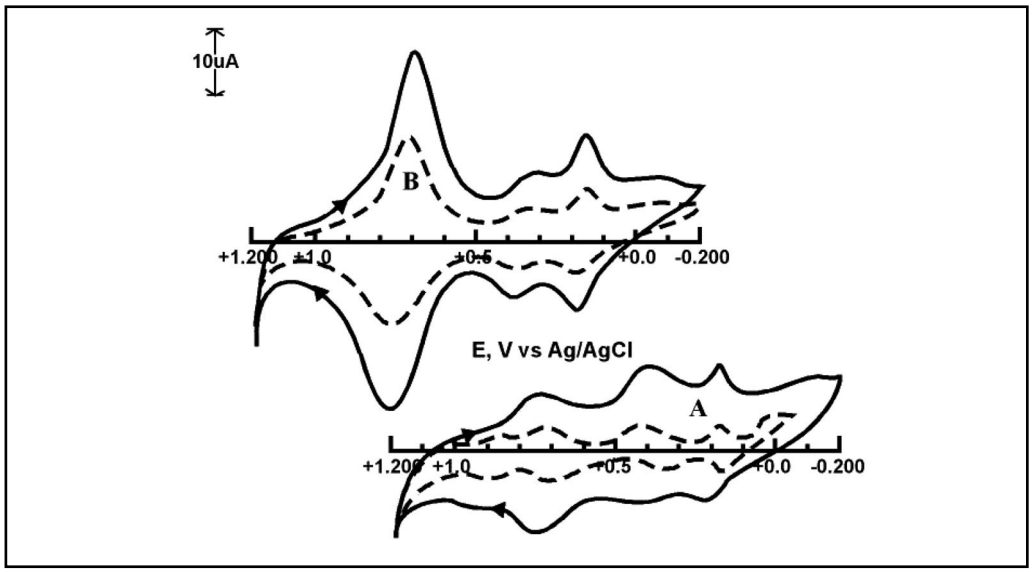

Fig. 6A Cyclic voltammogram of a GCE modified with Prussian blue under $K_xFe_y[Ir(CN)_6]_z$ in KCl/HCl
6B Cyclic voltammogram of a GCE modified with $K_xFe_y[Ir(CN)_6]_z$ under Prussian blue in KCl/HCl.
Scan rates: (----) at 0.005 V s^{-1}, (—) at 0.01V s^{-1}

obtained for a modified GCE with an assembly of $K_xFe_y[Fe(CN)_6]_z$ (Prussian blue) as the inner layers and $K_xFe_y[Ir(CN)_6]_z$ as the outer/upper layers in a 1:1 ratio (equal surface coverage of 1.97×10^{-9} mol cm^{-2}). The redox waves of the Ir-related centres overlap with that of the central Fe atom in Prussian blue at 0.75 V. The redox wave at 0.20 V is due to the counter Fe atom in the Prussian blue inner layer, while the redox wave of the counter Fe atom in the upper layer has an ill-developed anodic peak at 0.4 V. The fact that this redox wave exists suggests that the counter Fe ions in this assembly have two different redox potentials depending upon the central ion with which they associate. Due to the structure of the bi-film (which includes both Ir and Fe as central ions) two redox potentials of central Fe and Ir ions coexist and overlap. Figure 6B shows the cyclic voltammogram obtained for a modified GCE with an assembly of $K_xFe_y[Ir(CN)_6]_z$ as the inner layers and $K_xFe_y[Fe(CN)_6]_z$ (Prussian blue) as the outer/upper layers in a 1:1 ratio.

The order in which the layers are placed or formed affects the magnitude of the capacitive current. It also affects the shape of the collective redox waves in the assembly with very little change in the formal potentials of these redox waves, as observed when comparing the cyclic voltammograms in Figures 6A and 6B. The fact that the redox wave at ~ 0.75 V is much larger in Figure 6B than in Figure 6A may indicate that the upper $K_xFe_y[Ir(CN)_6]_z$ layer is more porous than Prussian blue. This will allow more transport of ions needed for electrical neutrality when both the central ions in Prussian blue and $K_xFe_y[Ir(CN)_6]_z$ are oxidised or reduced. The cyclic voltammogram for the film assembly created indicates perfect surface waves with smaller double layer capacitive current.

Evidence of Catalytic Activity

The catalytic activity of $K_xFe_y[Ir(CN)_6]_z$ was tested using the IO_3^- as a soft base with +7 oxidation state iodine atom. There was no technological significance behind the choice of that anion in this study. Modified GCEs with thin films of $K_xFe_y[Ir(CN)_6]_z$ exhibited electrocatalytic activities towards the reduction/oxidation of IO_3^-. Evidence for such catalytic behaviour can be seen in the cyclic voltammograms obtained in an acidic solution of KIO_3 (E°_f = 0.4 V vs. Ag/AgCl), see Figure 7A. A carbon paste electrode of the same apparent geometrical area was used to confirm

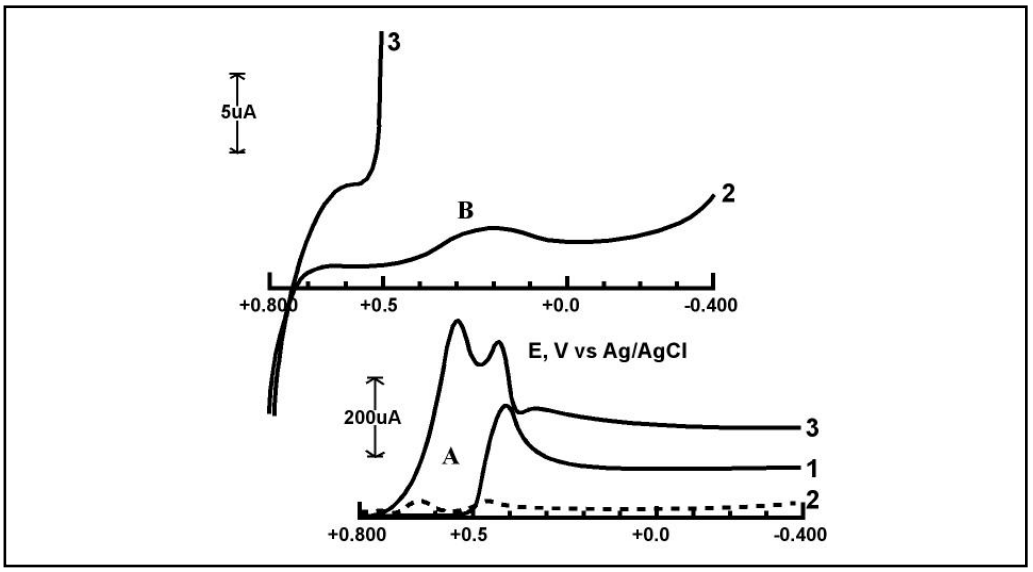

Fig. 7 Electrolytic catalytic activities towards the reduction of IO_3^- in aqueous KCl (pH = 1); scan rate 0.01 V s^{-1}
*7**A** 1 Naturally occurring/Native GCE in 0.05 M KIO_3 (KCl/HCl)*
2 GCE modified with $K_xFe_y[Ir(CN)_6]_z$ in KCl/HCl
3 GCE modified with $K_xFe_y[Ir(CN)_6]_z$ in 0.05 M KIO_3
*7**B** 2 GCE modified with $K_{x-1}Rh_yFe[Ir(CN)_6]_z$ in KCl/HCl*
3 GCE modified with $K_{x-1}Rh_yFe[Ir(CN)_6]_z$ in 0.5 M KIO_3

that the reduction peaks shown in Figure 6 were not due to an increase in electrode surface area.

Native GCE shows a reduction peak at 0.430 V (Figure 7A, line 1) whereas modified GCE with $K_xFe_y[Ir(CN)_6]_z$ (Figure 7A, line 3) shows reduction peaks with greater cathodic currents at 0.6 and 0.45 V. The larger cathodic current is due to the catalytic effect of $K_xFe_y[Ir(CN)_6]_z$. Furthermore, doping the film with an element from the same group as Ir (Rh) did not improve the catalytic activity. This can be concluded from Figure 7B (line 3), which represents the behaviour of GCEs modified with $K_{x-1}Rh_yFe[Ir(CN)_6]_z$ under the same experimental conditions. It can be noted that less catalytic current is generated from doped film than from undoped film. The observed catalytic current in Figure 7 is due to the reduction of iodate to iodide according to the Equation:

$$IO_3^- + 6H^+ + 6e \rightarrow I^- + 3H_2O \qquad \text{(iii)}$$

Conclusions

This study shows evidence of the efficient manipulation of Ir-HCM film structures to a desired composition and porosity. The redox behaviour of thin films of iridium-based HCMs differs from those of (3*d*) and (4*d*) metals-based HCM. The formation of higher oxidation state oxides in proximity to cyanide complexes was noticed with (3*d*) or (4*d*) metals. This was not the case for Ir-based HCM. The expanded valence shell of the Ir ion in which its (5*d*) electrons are preceded by $4f^{14}$ create a soft acid nature for Ir (II or III) ions as a central atom. The reactivity of its 6-π acceptor ligand (CN^-) with Ir ions may be considered when comparing the redox behaviour of (5*d*) metal-based HCM with those of (3*d*) or (4*d*) metal-based HCMs. The catalytic activity of Ir-based HCM agrees with that of most of the studied HCM and can be explained on the basis of an electron/proton transfer process.

References

1 Z. Gao, G. Wang, P. Li and Z. Zhao, *Electrochim. Acta*, 1991, **36**, 147
2 K. Itaya, H. Akahoshi, and S. Toshima, *J. Electrochem. Soc.*, 1985, **128**, (7), 1498
3 L. M. Siperko and T. Kuwana, *J. Electrochem. Soc.*, 1983, **130**, 396
4 V. D. Neff, *J. Electrochem. Soc.*, 1978, **125**, 886

5 K. K. Kasem, *J. Appl. Electrochem.*, 1999, **29**, 1473

6 T. R. Cataldi, C. E. de Benedetto and C. Campa, *J. Electroanal. Chem.*, 1997, **437**, 93

7 K. K. Kasem, *Mater. Sci. Eng.*, 2001, **B83**, 97

8 A. Dostal, M. Hermes and F. Scholtz, *J. Electroanal. Chem.*, 1996, **415**, 133

9 S. J. Reddy, A. Dostal and F. Scholtz, *J. Electroanal. Chem.*, 1996, **403**, 209

10 K. Kasem, R. Hazen and R. M. Spaulding, *Interface Sci.*, 2002, **10**, 261

11 D. Olaf, L. Sabine, H. Frank and B. Michael. *J. Exp. Bot.*, 1990, **41**, (230), 1055

12 L. Hartwig and B. Michael, *Plant Physiol.*, 1988, **86**, (4), 1044

13 K. K. Kasem, *J. Appl. Electrochem.*, 2001, **31**, 1125

14 S. Ohkoski, A. Fujishima and K. Hashimoto, *J. Am. Chem. Soc.*, 1998, **120**, 5349

15 J. A. Cox and R. K. Kulkarni, *Talanta*, 1986, **33**, (11), 911

16 J. A. Cox. and P. J. Kulesza, *Anal. Chem.*, 1988, **5**, (16), 1021

17 J. A. Cox, *J. Electroanal. Chem.*, 1987, **233**, (1–2), 87

18 P. J. Kulesza, *J. Electroanal. Chem.*, 1987, **220**, (2), 295

19 T. R. Cataldi, C. E. De Benedetto and C. Campa, *J. Electroanal. Chem.*, 1998, **458**, 149

20 Y. Wang, G. Zhu and E. Wang, *J. Electroanal. Chem.*, 1997, **430**, 127

21 J. P. Eaton and D. Nicholls, *Transition Met. Chem.*, 1981, **6**, 203

22 N. M. Pinhal and N. V. Vugman, *Hyperfine Interactions*, 1989, **52**, (1), 89

23 N. V. Vugman and N. M. Pinhal, Inst. Fis., Rio de Janeiro Univ., Brazil, Report, 1983, (UFRJ-IF-10/83), AN (1984) 166787

24 N. V. Vugman and N. M. Pinhal, *Mol. Phys.*, 1983, **49**, (6), 1315

25 N. V. Vugman, R. P. A. Muniz and J. J. Danon, *J. Chem. Phys.*, 1972, **57**, (3), 1297

26 K. Kasem, F. R. Steldt, T. J. Miller, and A. N. Zimmerman, *Microporous Mesoporous Mater.*, 2003, **66**, 133

27 W. Gorski and J. A. Cox, *Anal. Chem.*, 1994, **66**, 736

28 W. Sun, H. Liu, J. Kong, G. Xie and J. Deng, *J. Electroanal Chem.*, 1997, **437**, 67

29 K. Kasem and F. A. Schultz, *J. Inorg. Organomet. Polym.*, 1994, **4**, (4), 377

The Authors

Kasem K. Kasem is a Professor of Chemistry at Indiana University Kokomo, U.S.A. He is interested in developments in the field of applied electrochemistry, especially in physical and analytical applications of chemically-modified electrodes. He also has interests in semiconductor electrochemistry, the electrochemical behaviour of polymeric thin films, activation and metallisation of polymers, and the electrodeposition of metals and alloys.

Leslie Huddleston was an undergraduate at Indiana University Kokomo, U.S.A. when she worked on this project. She obtained her BS in chemistry at Kokomo and is currectly working in industry.